Relaxation of Alignment Errors and Phase Calibration in Computational Frequency-Diverse Imaging using Phase Retrieval

Published in:
IEEE Access

Document Version:
Publisher's PDF, also known as Version of record

Queen's University Belfast - Research Portal:
Link to publication record in Queen's University Belfast Research Portal

Relaxation of Alignment Errors and Phase Calibration in Computational Frequency-Diverse Imaging using Phase Retrieval

OKAN YURDUSEVEN [ID] **[1,2], (Senior Member, IEEE), THOMAS FROMENTEZE[3], AND DAVID R. SMITH[1], (Senior Member, IEEE)**
[1]Department of Electrical and Computer Engineering, Duke University, Durham, NC 27708, USA
[2]Jet Propulsion Laboratory, California Institute of Technology, Pasadena, CA 91106, USA
[3]Xlim Research Institute, University of Limoges, 87060 Limoges, France

Corresponding author: Okan Yurduseven (okan.yurduseven@jpl.nasa.gov)

ABSTRACT We demonstrate a computational, frequency-diverse, phaseless imaging technique at microwave frequencies that minimizes the impacts of phase calibration and alignment errors on image reconstruction. Phase calibration error is introduced by means of misaligning the sub-antennas forming an aperture, causing unwanted phase shifts between the forward model and adjoint operation. It is shown that by leveraging phase retrieval techniques, distinguishable images can still be reconstructed in the presence of significant phase errors, while complex-based reconstructions—those relying on measurement of both phase and amplitude—produce heavily corrupted images. Using a frequency-diverse imaging system consisting of a cavity-backed metasurface antenna that operates at microwave frequencies in the K-band (17.5–26.5 GHz), we demonstrate the complex-based and phaseless images of various objects, from a simple subwavelength conducting element to more complex metal structures. We verify that the combination of the phase retrieval approach with the frequency-diverse imager significantly improves the robustness of the composite imaging system to phase errors. While frequency-diverse computational imaging systems have significant advantages in terms of hardware, their reliance on a near-exact forward model places heavy requirements on system calibration. The phase retrieval approach developed here has the potential to alleviate this reliance, increasing the feasibility of such systems.

INDEX TERMS Microwaves, imaging, phase retrieval, computational imaging, coherent imaging, phase coherence, phaseless imaging, calibration, frequency-diversity.

I. INTRODUCTION

Electromagnetic (EM) imaging using microwaves, millimeter-waves (mmW) and sub-millimeter (THz) waves, offers significant advantages, including penetrating many optically opaque materials with non-ionizing radiation. These advantages make such modalities suitable for use in a wide range of applications, from security-screening [1]–[5] to non-destructive testing [6]–[8], through-wall imaging [9]–[11] and biomedical imaging [12]–[15].

Computational imaging is a modern imaging approach that shifts the design emphasis from system hardware to image processing and software, allowing alternative and innovative aperture concepts to be introduced. Such alternative platforms have the potential to yield lower-cost, high-performance imaging systems with advantages beyond conventional

systems [16]–[21]. Computational imaging architectures are increasingly attractive given the continual advances in computing power and capabilities, including parallel computing, field programmable gate arrays (FPGAs) and general-purpose computing on graphics processing unit (GPGPUs).

Frequency-diverse imaging is a computational imaging technique that leverages frequency-diverse antennas to capture and reconstruct scene information [22]–[42]. A frequency-diverse antenna radiates field patterns that vary strongly as a function of the driving frequency. Over a given frequency bandwidth, the fields of a frequency-diverse antenna vary spatially in a quasi-random (or quasi-orthogonal) manner across the operating frequency-band. The key feature of frequency-diverse imaging is that the scene information is encoded onto these quasi-random field

patterns, with the data acquired by means of a simple frequency sweep. Therefore, data-acquisition is performed in an all-electronic manner (no mechanical scanning apparatus is required) without the need for phase shifting circuits.

System calibration and phase errors can play a crucial role in frequency-diverse imaging [35]. This statement is also accurate for any imaging system, especially those systems operating in the radiating near-field (or Fresnel zone), regardless of the type of the imaging technique. For example, achieving the phase calibration of a sparse-array imaging system with electronic switches is presented in detail in [43]. In [44], a backscatter calibration technique using a modulated UWB calibration fiducial operating at K-band frequencies is demonstrated. System calibration and phase errors for imaging systems are of vital importance because coherent measurement of the object scattered fields (amplitude and phase) is strongly affected by the accuracy of the phase coherency achieved across the synthesized aperture. Possible factors degrading the phase coherency include poor characterization of the RF cables and connectors in the system and positional misalignment of the antennas in space, resulting in unwanted phase shifts that, when not corrected, can destroy the reconstructed images. As a result, phase calibration of a frequency-diverse system is vital to achieve successful imaging from such systems. Several techniques to achieve system calibration have been presented previously [35], [36].

Maintaining phase coherency across a synthesized aperture through calibration techniques is a challenging task. One potential technique to relax the phase coherency requirement would be the integration of the frequency-diverse technique with phase retrieval techniques, leading to phaseless computational imaging as described in [25] and [26]. Phase retrieval in conventional microwave and millimeter-wave SAR imaging and diagnostics has been demonstrated with promising results in the literature. These works include the use of indirect microwave holography [45], [46], the hybrid inexact Newton Method [47] and the combination of the Gerchberg-Saxton algorithm with the Misell algorithm [48].

In the present work, we demonstrate that by levering phase retrieval techniques, the effect of phase errors on reconstructed images can be reduced significantly, simplifying the calibration process required for imaging. The use of the frequency-diverse aperture within the system shown in this work enables the entire scene to be imaged using a single antenna by means of a simple frequency-sweep. As a result, the presented work brings the merits of the concepts of computational frequency-diverse imaging [22]–[42] and phase retrieval [25], [26], [45]–[48].

It should be emphasized that the contribution of this work is not to show frequency-diverse imaging and/or phase retrieval. Both these aspects have been covered in great detail in the literature. The novel contribution of this work is that this is the first time in the literature that the idea of leveraging the phase retrieval concept to address the system phase calibration requirement, a significant challenge within the imaging community, is demonstrated. The outcome of this work can be useful not only to the computational imaging community but also to the entire imaging community, especially within the field of near-field imaging, at microwave, millimeter-wave and submillimeter-wave frequencies. We also emphasize that while the use of the Wirtinger Flow phase retrieval algorithm enables us to leverage the scene sparsity, improving the convergence of the phase retrieval algorithm as we have demonstrated in [26], the presented concept in this work has the advantage to be generalized for any other phase retrieval algorithms and imaging modalities.

This paper is organized as follows: In Section II, we provide a brief description of the frequency-diverse imaging concept and its integration with the phase retrieval problem. Section III presents the imaging results, which confirm the importance of the phase retrieval technique to ease the phase accuracy requirement to achieve successful imaging. Finally, Section IV provides the concluding remarks.

II. FREQUENCY-DIVERSE IMAGING AND PHASE RETRIEVAL

A frequency-diverse imaging system makes use of one or more frequency-diverse antennas that produce spatially varying radiation patterns as a function of frequency. The field scattered from a given illumination pattern constitutes a measurement, such that the information content of a scene can be encoded onto a finite set of measurements indexed by frequency. From this measurement set, an estimate of the scene is reconstructed using computational imaging algorithms. The measured signal is related to the susceptibility (or reflectivity) distribution of the scene through the following equation, known as the *forward model*:

$$\mathbf{g}_{Mx1} = \mathbf{H}_{MxN}\mathbf{f}_{Nx1} + \mathbf{n}_{Mx1} \quad (1)$$

where $\mathbf{g}$ is the measurement vector, $\mathbf{H}$ is the measurement (or sensing) matrix, $\mathbf{f}$ is the scene reflectivity (or contrast) vector to be reconstructed and $\mathbf{n}$ is the measurement noise. The number of measurement modes is given by M while the scene is discretized into N diffraction-limited voxels. Here, we use bold font to denote the vector-matrix notation. Using the first Born approximation, the measurement matrix, $\mathbf{H}$, can be calculated as the dot product of the fields radiated by the transmit ($\mathbf{E}_{Tx}$) and receive ($\mathbf{E}_{Rx}$) frequency-diverse antennas that constitute the composite aperture, both of which are propagated to all points within the scene; $\mathbf{H}_{i,j}(w) = \mathbf{E}_{Tx}^{i}(w)\mathbf{E}_{Rx}^{j}(w)$, where w denotes the frequency, and i and j refer to the ith transmit and j^{th} receive antennas, respectively.

Fig. 1 depicts a generic imaging scenario where an antenna source, ρ_{Tx} (transmit mode) and ρ_{Rx} (receive mode), illuminates a scene and receives the reflected signal from the scene.

In Fig. 1, the antenna and the scene are represented by the coordinates $\mathbf{r}$ ($x = 0$, y, z) and $\mathbf{r}'$ (x', y', z'), respectively. Throughout this work, we restrict the polarization of the fields to a single linear polarization state, such that we can make
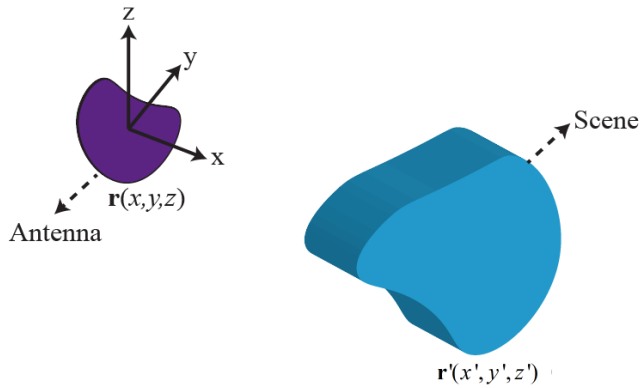
FIGURE 1. Depiction of a generic imaging scenario.

use of the scalar wave equation and propagator. From EM theory, it is well-known that the fields radiated from a source to a scene can be calculated using the Green's function [27], where the Green's function can be denoted as $G(\mathbf{r}, \mathbf{r}'; w) = \frac{e^{-jk_0|\mathbf{r}-\mathbf{r}'|}}{4\pi|\mathbf{r}-\mathbf{r}'|}$ for the scenario depicted in Fig. 1, where k_0 is the wavenumber in free-space. This statement suggests that the antenna sources are known through a characterization process. As an example, in the experimental portion of the work presented here, the characterization of the antenna aperture fields is performed using a planar near-field scanning system, NSI 200V-3x3 [31], [36]. After the characterization within the near-field scanning apparatus, the characterized antennas must be relocated and integrated into the imaging aperture—a process that, when not carefully handled, results in misalignment errors, giving rise to unwanted phase errors in the forward model.

The underlying reason as to why the complex-based (amplitude and phase) reconstruction can be significantly affected by phase errors can be understood by analyzing the amplitude and phase response of the Green's function in the presence of a phase error. Let us assume a phase characterization error for the scenario depicted in Fig. 1 by introducing a misalignment to the calculation of the **H**-matrix. This effectively translates into adding a phase distortion to the Green's function. As an example, let us consider a physical misalignment in the position of the antenna by a factor of $\lambda_0/10$, which may seem a relatively small physical displacement. This means that while the measurements (**g**) are taken at a $\lambda_0/10$ offset from the correct (or reference) distance – corresponding to the left side of (1) – the phase of the **H**-matrix on the right side of (1) is calculated with respect to the reference distance, corresponding to a phase shift of $e^{(-j\frac{2\pi}{\lambda_0}\frac{\lambda_0}{10})} e^{(-j\frac{2\pi}{\lambda_0}\frac{\lambda_0}{10})} = e^{(-j\frac{4\pi}{\lambda_0}\frac{\lambda_0}{10})}$, or 72°, between both sides of (1) which can easily distort the image reconstruction, especially for systems where multiple transmit and receive antennas are present with each antenna exhibiting a different phase error. This gives rise to the conclusion that the forward model of (1) requires maintaining extremely accurate phase coherency for the high-fidelity reconstruction.

The measurement of the object scattered fields, given as **g** in (1), is achieved through the forward model. The reconstruction of the scene (including the imaged object), given as **f** in (1), is known as the adjoint operation. Both these terms, forward model and adjoint operation, will be used frequently throughout this paper to explain the concept of phase error (or poor phase coherency). We note that, as mentioned earlier, in practice, there can be several possible factors degrading the phase coherence accuracy of an imaging system, from poor calibration of the RF cables and connectors to positional misalignments of the antennas. In this work, the concept of phase error is studied by means of antenna position misalignments.

Considering the forward model and adjoint (or reconstruction) operation, it is possible to look at an imaging problem as a two-step process. The first step involves the measurement of the object scattered fields (forward model) while the second step involves reconstructing an estimate of the scene using the measured object scattered fields (adjoint operation). As a result, for an imaging system, we can have two system layout definitions; one for the forward model and another one for the adjoint operation. Here, the term system layout refers to the positions of the antennas within the imaging system. Ideally, it is desired that these two layouts are identical, suggesting that no phase error caused by antenna misalignments is present between the forward model and adjoint operation. Let us now consider an imaging system consisting of misaligned antennas (system layout definition for the forward model). When the antennas in such a system measure the object scattered fields, the phase information encoded in the measured signal will be governed by the positions of the misaligned antennas. If we do not know that the antennas are misaligned, which is typically the case, and calculate the adjoint operation assuming that the antennas are correctly aligned (system layout definition for the adjoint operation), then a phase error in the forward model with respect to the adjoint operation is present, which, as will be shown later, can easily destroy the reconstructed images when imaging is done in a conventional, complex-based (amplitude and phase) manner. It should be noted that imaging in the K-band is a wideband problem, suggesting that a physical misalignment would produce different phase offsets as the operating frequency is swept within the K-band. As a result, when reporting the phase errors caused by a physical antenna misalignment, we take the center frequency within the K-band, 22 GHz, as a reference.

The conventional way of solving (1) for an estimate of the scene reflectivity vector, $\mathbf{f}_{est}$, involves using various computational imaging algorithms, from the single-shot matched filter technique to iterative least-squares based methods [30]. Different from complex-based (1), leveraging phase retrieval techniques, $\mathbf{f}_{est}$ is reconstructed from intensity-only measurements of the signal scattered from the object, $|\mathbf{g}|^2$, resulting in solving the following equation to recover $\mathbf{f}_{est}$

$$\mathbf{g}_{int} = |\mathbf{g}|^2 = |\mathbf{H}\mathbf{f} + \mathbf{n}|^2 \qquad (2)$$

A number of phase retrieval techniques can be adapted to solve (2) for $\mathbf{f}_{est}$, including the block-Kaczmarz method [49] and the Wirtinger Flow technique [25], [26]. Building on our recent works on phase retrieval in computational frequency-diverse imaging problems [25], [26], we use here the Wirtinger Flow algorithm. The Wirtinger Flow technique relies on an iterative gradient-descent based algorithm to retrieve phase information from phaseless, intensity-only measurements of the scene, which can significantly reduce the effect of phase errors on image reconstruction. To put this statement into context, let us consider the same phase error example provided for the complex-based imaging problem earlier. Adding a misalignment factor of $\lambda_0/10$, corresponding to a total pure phase error of 72° from the Green's functions of the transmit and receive paths, causes only a weak perturbation on the intensity of the right side of (2); a variation happening much more slowly than the phase for the same displacement. Phaseless imaging involves minimizing the distance between the intensities of the calculated measurement vectors at each iteration, which is inherently robust to the phase errors added to the **H**-matrix. As a result, the effect of phase coherence accuracy on image reconstruction can be reduced significantly in comparison to conventional complex-based reconstructions.

III. IMAGING RESULTS AND DISCUSSION

A. SAR IMPLEMENTATION

For imaging systems relying on phase coherency, system phase calibration is of vital importance to achieve imaging. To put this statement into context, we first study a conventional synthetic aperture radar (SAR) problem. For this study, we synthesize a composite aperture, 5 cm x 5 cm, using an open-ended waveguide probe antenna as depicted in Fig. 2(a). The antenna is mechanically raster scanned across the synthesized aperture at half-wavelength ($\lambda/2$) intervals, imaging a point scatter target. To reduce the size of the computational problem, imaging is performed at a single frequency, 22 GHz, selected to be within the K-band frequency regime, 17.5-26.5 GHz.

This study is performed using a MATLAB based, in-house developed simulation software, the Virtualizer [28]. The Virtualizer simulation tool enables us to synthesize any composite aperture of interest and perform critical imaging tasks using the synthesized aperture, including modeling of the antennas within the aperture, propagation of antenna radiated fields to the scene to be imaged, forward model and image reconstruction. Using the Virtualizer, the antennas can be modeled analytically or experimentally (by means of importing the NSI scanned near-field data into the Virtualizer).

The imaging is performed in two ways; (a) using complex-based (amplitude and phase) measurements and (b) intensity-only measurements. For both scenarios, imaging is done with and without phase errors added to the synthesized system. The addition of the phase error to the imaging problem is realized by means of creating a misalignment between the positions of the antenna for the forward model and the adjoint
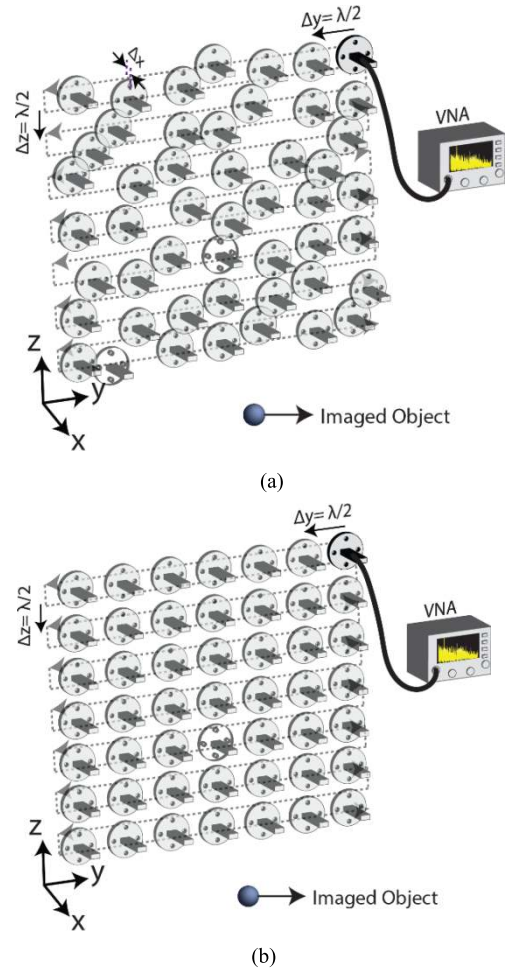
FIGURE 2. Depiction of the synthesized SAR aperture imaging a point scatter. The phase error is added by means of misaligning the antenna (in x-axis or range) for the forward model (a) layout for the forward model (misaligned – denoted by Δx) (b) layout for the adjoint operation (calculated for correct alignment).

(or reconstruction) operation as shown in Figs. 2(a) and 2(b). This process will be explained in detail in Section III.B; our purpose here is to show the effect of phase errors on imaging for a conventional SAR scenario. By imaging a point scatter, we obtain the transfer function of the system by means of a point-spread-function (PSF) analysis. This study is important in that analyzing the PSF of an imaging system can serve as a good metric in understanding the effect of phase errors on image reconstruction. Fig. 2 depicts the synthesized SAR system together with the imaged point scatter target.

For the ideal scenario, no phase error is added to the measurements (no antenna position misalignment is present between the forward model and adjoint operation). The complex-based reconstructed image (or the PSF pattern) for this scenario is shown in Fig. 3(a). The PSF pattern shown in Fig. 3(a) is extremely clean and exhibits good fidelity. Following the ideal scenario, we image the same point scatter target using the same SAR aperture but add a random phase error to the measured data (forward model) by means of misaligning the antenna in range (x-axis) at each
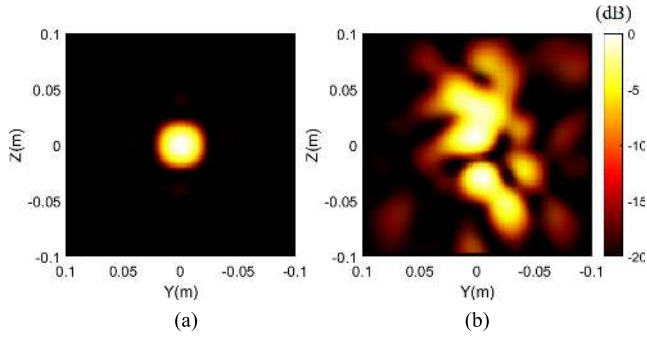
FIGURE 3. Complex-based SAR reconstructed PSF patterns (a) without phase error (b) with phase error.

FIGURE 5. Synthesized frequency-diverse imaging system (a) side-view showing the front metasurface layer and the imaging stage (b) back-view showing the ports of the antenna.

sampling point as shown in Fig. 2(a). The added phase error is within the range of 0° and 180°, with a mean value of 65°. The complex-based phase corrupted PSF pattern is shown in Fig. 3(b). It is evident that the PSF pattern in Fig. 3(b) is heavily corrupted, exhibiting strong sidelobes. Figs. 3(a) and 3(b) visually underscore the importance of maintaining accurate phase coherency across the synthesized aperture when complex-based measurements are used for imaging.

Following the coherent SAR scenario, we study the implementation of phase retrieval in SAR imaging. The phase retrieval technique is Wirtinger Flow algorithm, relying on a gradient-descent based iterative scheme to solve the phaseless imaging problem [25], [26]. For this study, we use the same SAR system shown in Fig. 2. Similar to the complex-based coherent SAR imaging scenario studied in Fig. 3, imaging is done with and without phase errors added to the system. The amount of phase error is identical to the phase error studied for the complex-based problem in Fig. 3(b). The phaseless reconstructed PSF patterns are shown in Figs. 4(a) and 4(b).
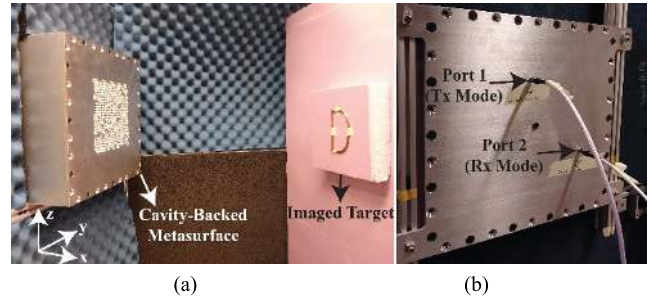

FIGURE 4. Phaseless SAR reconstructed PSF patterns (a) without phase error (b) with phase error.

Analyzing Fig. 4, it is evident that the effect of phase error on image reconstruction is significantly reduced as a result of adopting the phase retrieval technique.

B. FREQUENCY-DIVERSE COMPUTATIONAL IMAGING

Following the SAR studies, we present the implementation of phase retrieval for computational frequency-diverse imaging modalities to improve the phase error robustness

of such systems for imaging. The synthesized frequency-diverse imaging system for this study is illustrated in Fig. 5. The frequency-diverse imager consists of a cavity-backed frequency-diverse antenna with a metasurface layer radiating quasi-random field patterns across the K-band frequency spectrum.

The metasurface layer consists of subwavelength irises distributed across the antenna aperture in a random fashion while the cavity-backed structure is excited through two ports; port 1 for the transmit mode and port 2 for the receive mode. Both ports are connected to a vector network analyzer (VNA) (Agilent N5245A). Although the phase retrieval does not require vector measurement equipment for imaging, the VNA enables us to present the complex-based reconstructions for comparison.

In frequency-diverse imaging, an important factor determining the orthogonality of the measurement modes is the quality (Q) factor of the frequency-diverse antennas. Increasing the Q-factor improves the orthogonality of the measurement modes, reducing the information redundancy. We analyze the Q-factor of the cavity-backed metasurface antenna from the time-domain impulse response [23] and report it to be $Q = 12000$, suggesting that the cavity-backed metasurface antenna can produce up to 4900 modes (upper-bound limit), calculated using the theory presented in [22]. In this work, the K-band is sampled at 4001 frequency points, corresponding to a frequency interval of $\Delta f = 2.25$ MHz, satisfying the calculated theoretical upper-bound limit.

Using the synthesized frequency-diverse system shown in Fig. 5, we first image a point scatter target as depicted in Fig. 6 and analyze the PSF characteristics. First, imaging is performed in the absence of phase errors, suggesting that system phase calibration and antenna alignment are ideal. PSF imaging is performed in two ways; (a) using the complex-based (amplitude and phase) scattered signal as in (1), and (b) using the phaseless, intensity-only scattered signal as in (2). The reconstructed PSF patterns are shown in Fig. 7.

The complex-based reconstruction shown in Fig. 7(a) uses a single-shot matched filter reconstruction technique to recover the estimate of the scene, $\mathbf{f}_{est} = \mathbf{H}^{\dagger}\mathbf{g}$, where $\mathbf{H}^{\dagger}$ denotes the complex conjugate transpose of the **H**-matrix [30]. The phaseless reconstruction in Fig. 7(b),
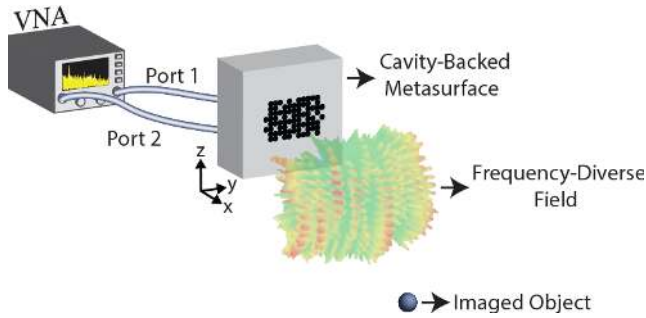
FIGURE 6. Imaging of a point target using the frequency-diverse system.

FIGURE 8. Addition of the phase error by means of position misalignment of the frequency-diverse antenna when calculating the Hmatrix. The transmit fields are calculated with a *x* = 2 cm offset while the receive fields are calculated with a *x* = 10 cm offset in range.
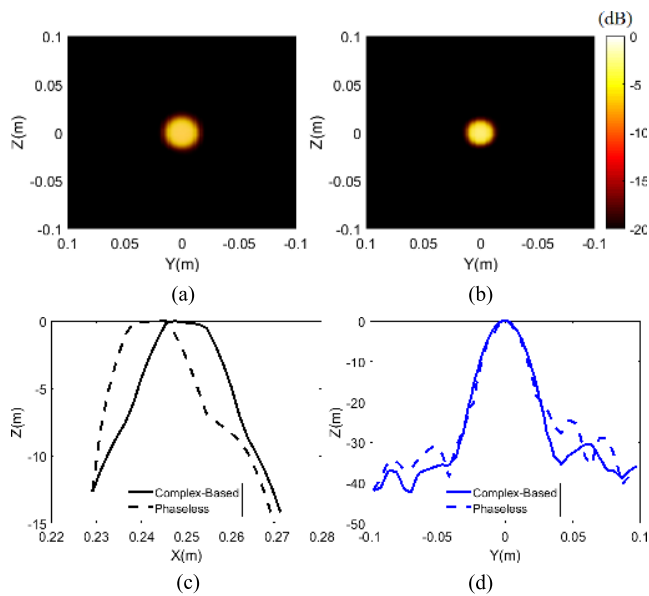

FIGURE 7. Reconstructed PSF patterns (a) complex-based reconstruction (b) phaseless intensity-only reconstruction (c) comparison in range (d) comparison in cross-range. No phase error is present.

on the other hand, runs an iterative gradient-descent based solver to recover $\mathbf{f}_{est}$ from (2) [25], [26]. It should be noted that although the reconstructed PSF patterns are 3D, in Figs. 7(a) and (b), we demonstrate the front projections (*yz*-plane) of the reconstructions. A comparison of the PSF patterns in range (*x*-axis) and cross-range (*y*-axis) are also shown in Figs 7(c) and (d), respectively. Analyzing Fig. 7, it is evident that both the complex-based and phaseless reconstructions produce well-defined, comparable PSF patterns in the absence of a phase error. The slight discrepancy between the complex-based and phaseless reconstructed PSF patterns in Fig. 7(c) can be attributed to the fact that the time delay information between the transmit and receive waveforms caused by the distance of the imaged object (giving rise to the phase information in the frequency domain) cannot be preserved in intensity-only measurements. Despite the absence of the direct phase data, the phase information is retrieved from intensity-only measurements to a good accuracy, with the difference between the peaks of the phaseless and complex-based reconstructed PSF patterns being less than 1 cm in range.
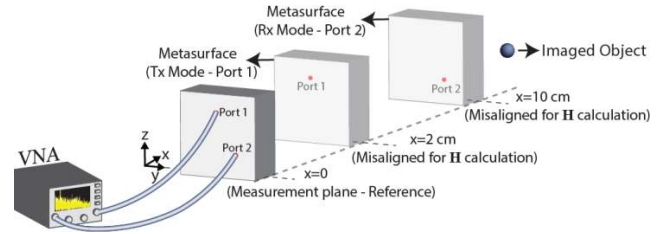
Next, we study a similar PSF imaging scenario but in the presence of a phase error added to the measurements. In this study, the phase error is added by deliberately misaligning the cavity-backed metasurface antenna when calculating the **H**-matrix for the forward model in (1) and (2). To introduce this error, as depicted in Fig. 8, into the calculation of transmit fields, $\mathbf{E}_{Tx}$, the antenna is misaligned by $x = 2$ cm in range while the fields from the receive mode, $\mathbf{E}_{Rx}$, are calculated with an $x = 10$ cm misalignment in range. It should be noted here that these misalignment errors are chosen as an example and similar analysis can be carried out for different misalignment configurations.

In this study, similar to the SAR scenarios studied earlier, we analyze the phase error caused by the position misalignment in the range direction (x-axis). For two given transverse planes close to each other along the x-axis, the magnitude can be almost the same while the phase exhibits rapid variation. The studied misalignment configuration translates to a phase error of around 100° for both the transmit (Tx) and receive (Rx) modes at the center frequency, 22 GHz, suggesting that a significant phase error is added to the forward model. In practice, such large phase errors might not be present; however, our aim here is to show that by encoding the phase information onto intensity-only measurements and implementing the phase retrieval technique, we can reduce the effect of phase errors on imaging even under such extreme conditions. The reconstructed PSF patterns are shown in Fig. 9.

Analyzing the PSF patterns presented in Fig. 9 reveals a significant advantage of the phaseless configuration. As shown in Fig. 9(a), the complex-based reconstruction is corrupted by the added phase error, presenting considerably increased sidelobes. The phaseless reconstructed PSF pattern in Fig. 9(b), on the other hand, is still of high-fidelity with significantly lower sidelobe levels in comparison to the complex-based reconstructed PSF pattern. Analyzing the PSF curves plotted in range (x-axis) – Fig. 9(c) – and cross-range (y-axis) – Fig. 9(d) – confirms this observation. A careful analysis of these results shows that the sidelobe levels for the complex-based reconstructed PSF patterns are as high as above -5 dB in range and above -10 dB in cross-range.

Following the PSF analysis, we turn our attention to imaging of more complicated targets. Using the synthesized frequency-diverse imager of Fig. 5, we image the letters
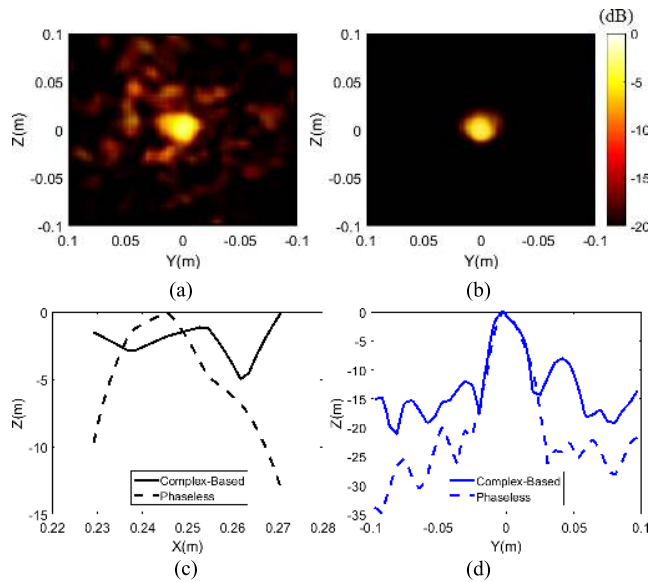
FIGURE 9. Reconstructed PSF patterns (a) complex-based reconstruction (b) phaseless intensity-only reconstruction (c) comparison in range (d) comparison in cross-range. Phase error is present.

"D", "U", "K" and "E", forming the word "DUKE". Similar to the PSF analysis, imaging is first performed for the ideal scenario exhibiting no phase errors in the system, suggesting an ideal system calibration and antenna position alignment. Imaging is performed in two ways; (a) matched-filter reconstruction using the complex-based **g** measurement vector (amplitude and phase) in (1) and (b) phaseless reconstruction using the intensity-only measurements, $|\mathbf{g}|^2$ in (2). The reconstructed images are shown in Fig. 10.

Analyzing Fig. 10, it can be seen that both the complex-based and phaseless reconstructions reveal a clear outline of the imaged objects. Following this ideal scenario, we perform the same study but in the presence of a phase distortion added to the imaging problem. Similar to the PSF analyses presented earlier, this is achieved by deliberately misaligning the frequency-diverse antenna ($x = 2$ cm in transmit mode and $x = 10$ cm in receive mode) when calculating the **H**-matrix in (1) and (2). The complex-based and phaseless reconstructed images of the same "DUKE" target are shown in Fig. 11.

Different from Fig. 10, in Fig. 11, there is a considerable difference between the complex-based and phaseless reconstructed images. Analyzing Fig. 11(a), it is evident that the complex-based reconstructed images are significantly corrupted by the introduced phase error and present no useful information. The phaseless reconstructed images shown in Fig. 11(b), on the other hand, although slightly distorted in comparison to Fig. 10(b), are still distinguishable. This suggests that even in the presence of such extreme phase errors, the phaseless reconstruction could still reconstruct a reliable estimation of the scene, suggesting a significant reduction in the required phase calibration tolerances.

The phaseless frequency-diverse computational imaging technique essentially encodes the phase information onto
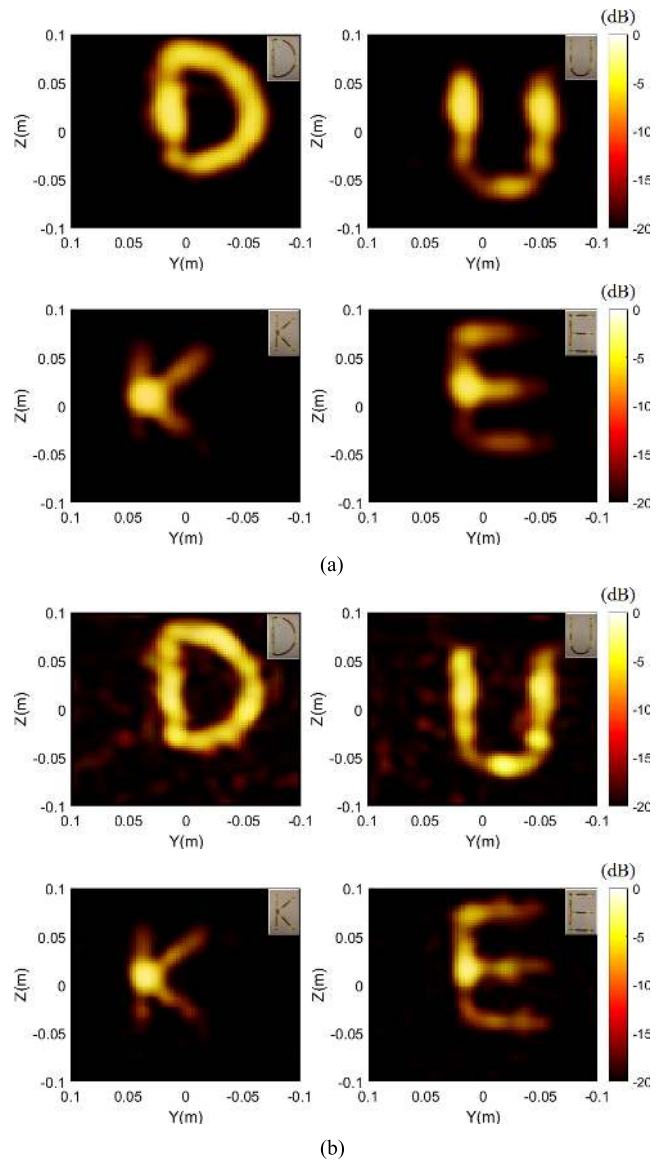
FIGURE 10. Reconstructed images of letters "DUKE" (a) complex-based reconstructions (b) phaseless intensity-only reconstructions. No phase error is present. Actual imaged objects are shown as insets.

a set of intensity-only measurements taken by means of a simple frequency-sweep. A significant advantage of leveraging the phase retrieval concept is that the effect of phase errors in the system is weaker on intensity-only data in comparison to the phase data. This is the underlying reason why the phaseless reconstructed images in Fig. 11(b) are still distinguishable while the complex-based reconstructed images in Fig. 11(a) are destroyed. We can prove this phenomenon by simply analyzing the measurement matrix, **H**, with and without the phase error. To this end, in Fig. 12, we plot the amplitude ($|\mathbf{H}|$) and phase ($\angle\mathbf{H}$) of the measurement matrix **H** at the center frequency within the K-band frequency regime, 22 GHz. Whereas the scenes imaged in Figs. 10 and 11 are 3D, for this study, we choose a single
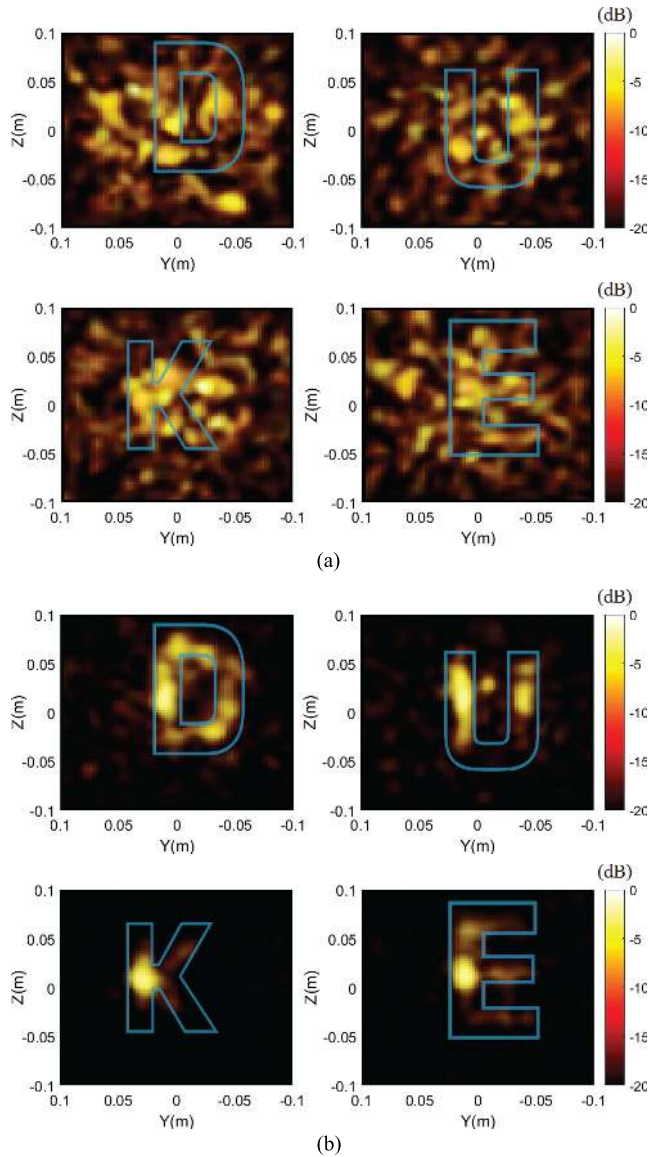
FIGURE 11. Reconstructed images of letters "DUKE" (a) complex-based reconstructions (b) phaseless intensity-only reconstructions. Outlines of the imaged letters are highlighted in blue color. Phase error is present.

slice within the 3D volume, such that that the patterns of the **H**-matrix in Fig. 12 are projections on a 2D plane. Recalling the description of the **H**-matrix given earlier, in Fig. 12 we are essentially evaluating the scalar product of the fields radiated by the metasurface antenna (transmit and receive) propagated to the selected 2D plane at a single frequency in the presence and absence of a phase error. The error is added to the Green's function propagator by means of a position misalignment as depicted in Fig. 8.

Analyzing Figs. 12(a) and (b), it can be seen that the effect of the added phase error on the amplitude data is weak, as confirmed by the amplitude difference pattern shown in Fig. 12(c). The phase patterns in Fig. 12(d) and (e), on the other hand, are significantly different, as highlighted by the phase difference plot shown in Fig. 12(f). Fig. 12,
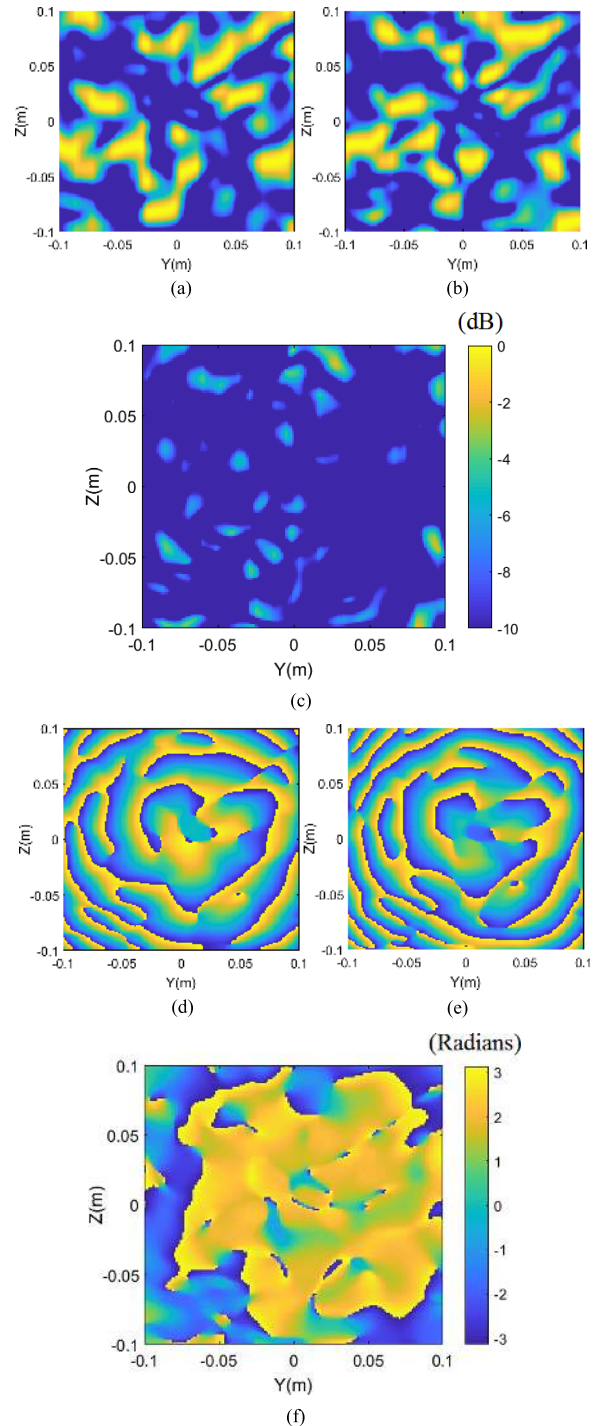
FIGURE 12. Effect of phase error on amplitude and phase of the measurement matrix, H. Amplitude (10 dB dynamic range); (a) without phase error (b) with phase error (c) amplitude difference pattern. Phase (radians); (d) without phase error (e) with phase error (f) phase difference pattern.

demonstrating the intensity-only robustness of the measurement matrix **H** to phase errors is also a testament of the robustness of the intensity-only measurements of the scene, $\mathbf{g}_{int}$, to phase errors in (2). As the scene estimate is essentially the correlation between **g** and **H**, this also proves the improved robustness of the reconstructed images to phase errors.

The results shown in Fig. 12 confirm that encoding the phase information onto intensity-only measurements to be retrieved using phase retrieval techniques is an effective method to reduce the effect of phase errors on imaging, an outcome that can significantly simplify the phase calibration process for imaging systems and ease the calibration tolerances to achieve imaging.

We note that for the imaging scenarios studied in Figs. 10 and 11, the data acquisition time is 1.53 seconds whereas imaging the same scene using a SAR system mechanically raster scanning the scene takes 10 minutes and 24 seconds. It should be noted that the data acquisition time for the SAR scenario can be drastically reduced by employing a populated aperture with an array of switching circuits. However, populating the same size aperture as the cavity-backed frequency-diverse metasurface antenna at the Nyquist limit would require $22 \times 22 = 484$ antennas whereas the frequency-diverse system uses a single antenna to encode the scene information. The image reconstruction time is reported to be 0.012 seconds for the complex-based matched filter reconstructions, slightly slower in comparison to using an FFT/inverse-FFT based SAR reconstruction technique, 0.01 seconds. The reconstruction time for the phaseless images is reported to be 6.6 seconds, an expected result due to the iterative nature of the phase retrieval algorithm as opposed to single-shot matched filter reconstructions.

IV. CONCLUSION

We have shown the application of phase retrieval in frequency-diverse computational imaging to improve the robustness of the imaging problem to phase errors, simplifying the phase calibration and alignment requirements for imaging. This is especially important for applications where maintaining phase coherency across large scanning apertures can be a difficult task. It has been verified that even under extreme phase distortions, the adoption of phase retrieval techniques makes it possible to recover distinguishable images for a variety of targets studied, from a simple point scatter target to a more complicated "DUKE" target. Phase retrieval also enables imaging by means of scalar measurements of the object scattered fields which can be taken using low-cost power meters and spectrum analyzers, significantly reducing the system cost. Although shown for the microwave spectrum, the presented technique can be adopted for imaging systems operating in the higher frequency spectra, including millimeter-wave and submillimeter-wave frequency regimes, where achieving accurate phase characterization is even more difficult due to the reduced wavelengths.

REFERENCES

[1] J. A. Martinez-Lorenzo, F. Quivira, and C. M. Rappaport, "SAR imaging of suicide bombers wearing concealed explosive threats," *Prog. Electromagn. Res.*, vol. 125, pp. 255–272, Feb. 2012.

[2] D. M. Sheen, D. L. McMakin, and T. E. Hall, "Three-dimensional millimeter-wave imaging for concealed weapon detection," *IEEE Trans. Microw. Theory Techn.*, vol. 49, no. 9, pp. 1581–1592, Sep. 2001.

[3] X. Zhuge and A. G. Yarovoy, "A sparse aperture MIMO-SAR-based UWB imaging system for concealed weapon detection," *IEEE Trans. Geosci. Remote Sens.*, vol. 49, no. 1, pp. 509–518, Jan. 2011.

[4] S. S. Ahmed, A. Genghammer, A. Schiessl, and L.-P. Schmidt, "Fully electronic *E*-band personnel imager of 2 m² aperture based on a multistatic architecture," *IEEE Trans. Microw. Theory Techn.*, vol. 61, no. 1, pp. 651–657, Jan. 2013.

[5] O. Yurduseven, "Indirect microwave holographic imaging of concealed ordnance for airport security imaging systems," *Prog. Electromagn. Res.*, vol. 146, pp. 7–13, Apr. 2014.

[6] S. Kharkovsky and R. Zoughi, "Microwave and millimeter wave nondestructive testing and evaluation—Overview and recent advances," *IEEE Instrum. Meas. Mag.*, vol. 10, no. 2, pp. 26–38, Apr. 2007.

[7] S. Caorsi, A. Massa, M. Pastorino, and M. Donelli, "Improved microwave imaging procedure for nondestructive evaluations of two-dimensional structures," *IEEE Trans. Antennas Propag.*, vol. 52, no. 6, pp. 1386–1397, Jun. 2004.

[8] R. Zoughi, *Microwave Non-Destructive Testing and Evaluation Principles*, vol. 4. Springer, 2012.

[9] T. S. Ralston, G. L. Charvat, and J. E. Peabody, "Real-time Through-wall imaging using an ultrawideband multiple-input multiple-output (MIMO) phased array radar system," in *Proc. IEEE Int. Symp. Phased Array Syst. Technol.*, Oct. 2010, pp. 551–558.

[10] S. Depatla, C. R. Karanam, and Y. Mostofi, "Robotic through-wall imaging: Radio-frequency imaging possibilities with unmanned vehicles," *IEEE Antennas Propag. Mag.*, vol. 59, no. 5, pp. 47–60, Oct. 2017.

[11] Y. Wang and A. E. Fathy, "Advanced system level simulation platform for three-dimensional UWB through-wall imaging SAR using time-domain approach," *IEEE Trans. Geosci. Remote Sens.*, vol. 50, no. 5, pp. 1986–2000, May 2012.

[12] N. K. Nikolova, "Microwave imaging for breast cancer," *IEEE Microw. Mag.*, vol. 12, no. 7, pp. 78–94, Dec. 2011.

[13] D. Kurrant, J. Bourqui, C. Curtis, and E. Fear, "Evaluation of 3-D acquisition surfaces for radar-based microwave breast imaging," *IEEE Trans. Antennas Propag.*, vol. 63, no. 11, pp. 4910–4920, Nov. 2015.

[14] M. J. Burfeindt, J. D. Shea, B. D. Van Veen, and S. C. Hagness, "Beamforming-enhanced inverse scattering for microwave breast imaging," *IEEE Trans. Antennas Propag.*, vol. 62, no. 10, pp. 5126–5132, Oct. 2014.

[15] M. Elsdon, O. Yurduseven, and D. Smith, "Early stage breast cancer detection using indirect microwave holography," *Prog. Electromagn. Res.*, vol. 143, pp. 405–419, Nov. 2013.

[16] D. Shrekenhamer, C. M. Watts, and W. J. Padilla, "Terahertz single pixel imaging with an optically controlled dynamic spatial light modulator," *Opt. Exp.*, vol. 21, no. 10, pp. 12507–12518, 2013.

[17] D. Shin, A. Kirmani, V. K. Goyal, and J. H. Shapiro, "Photon-efficient computational 3-D and reflectivity imaging with single-photon detectors," *IEEE Trans. Comput. Imag.*, vol. 1, no. 2, pp. 112–125, Jun. 2015.

[18] O. S. Cossairt, D. Miau, and S. K. Nayar, "Scaling law for computational imaging using spherical optics," *J. Opt. Soc. Amer. A, Opt. Image Sci.*, vol. 28, no. 12, pp. 2540–2553, 2011.

[19] D. J. Brady, *Optical Imaging and Spectroscopy*. New York, NY, USA: Wiley, 2009.

[20] M. F. Duarte *et al.*, "Single-pixel imaging via compressive sampling," *IEEE Signal Process. Mag.*, vol. 25, no. 2, pp. 83–91, Mar. 2008.

[21] S. S. Welsh, M. P. Edgar, R. Bowman, P. Jonathan, B. Sun, and M. J. Padgett, "Fast full-color computational imaging with single-pixel detectors," *Opt. Exp.*, vol. 21, no. 20, pp. 23068–23074, 2013.

[22] D. L. Marks, J. Gollub, and D. R. Smith, "Spatially resolving antenna arrays using frequency diversity," *J. Opt. Soc. Amer. A, Opt. Image Sci.*, vol. 33, no. 5, pp. 899–912, 2016.

[23] O. Yurduseven, J. N. Gollub, D. L. Marks, and D. R. Smith, "Frequency-diverse microwave imaging using planar Mills–Cross cavity apertures," *Opt. Exp.*, vol. 24, no. 8, pp. 8907–8925, 2016.

[24] J. Hunt *et al.*, "Metamaterial apertures for computational imaging," *Science*, vol. 339, no. 6117, pp. 310–313, Jan. 2013.

[25] T. Fromenteze, X. Liu, M. Boyarsky, J. Gollub, and D. R. Smith, "Phaseless computational imaging with a radiating metasurface," *Opt. Exp.*, vol. 24, no. 15, pp. 16760–16776, 2016.

[26] O. Yurduseven, T. Fromenteze, D. L. Marks, J. N. Gollub, and D. R. Smith, "Frequency-diverse computational microwave phaseless imaging," *IEEE Antennas Wireless Propag. Lett.*, vol. 16, pp. 2808–2811, 2017.

[27] G. Lipworth *et al.*, "Metamaterial apertures for coherent computational imaging on the physical layer," *J. Opt. Soc. Amer. A, Opt. Image Sci.*, vol. 30, no. 8, pp. 1603–1612, 2013.

[28] G. Lipworth *et al.*, "Comprehensive simulation platform for a metamaterial imaging system," *Appl. Opt.*, vol. 54, no. 31, pp. 9343–9353, 2015.

[29] J. Hunt *et al.*, "Metamaterial microwave holographic imaging system," *J. Opt. Soc. Amer. A, Opt. Image Sci.*, vol. 31, no. 10, pp. 2109–2119, 2014.

[30] O. Yurduseven *et al.*, "Resolution of the frequency diverse metamaterial aperture imager," *Prog. Electromagn. Res.*, vol. 150, pp. 97–107, Jan. 2015.

[31] T. Fromenteze *et al.*, "Computational imaging using a mode-mixing cavity at microwave frequencies," *Appl. Phys. Lett.*, vol. 106, no. 19, p. 194104, 2015.

[32] O. Yurduseven, V. R. Gowda, J. N. Gollub, and D. R. Smith, "Printed aperiodic cavity for computational and microwave imaging," *IEEE Microw. Wireless Compon. Lett.*, vol. 26, no. 5, pp. 367–369, May 2016.

[33] T. Fromenteze, O. Yurduseven, M. Boyarsky, J. Gollub, D. L. Marks, and D. R. Smith, "Computational polarimetric microwave imaging," *Opt. Exp.*, vol. 25, no. 22, pp. 27488–27505, 2017.

[34] O. Yurduseven, V. R. Gowda, J. N. Gollub, and D. R. Smith, "Multistatic microwave imaging with arrays of planar cavities," *IET Microw., Antennas Propag.*, vol. 10, no. 11, pp. 1174–1181, Aug. 2016.

[35] O. Yurduseven, J. N. Gollub, K. P. Trofatter, D. L. Marks, A. Rose, and D. R. Smith, "Software calibration of a frequency-diverse, multistatic, computational imaging system," *IEEE Access*, vol. 4, pp. 2488–2497, 2016.

[36] O. Yurduseven, J. N. Gollub, D. L. Marks, and D. R. Smith, "Alignment correction for antenna scans in imaging," in *Proc. IEEE Int. Symp. Antennas Propag., USNC/URSI Nat. Radio Sci. Meeting*, San Diego, CA, USA, Jul. 2017, pp. 2381–2382.

[37] O. Yurduseven, D. L. Marks, J. N. Gollub, and D. R. Smith, "Synthesizing a frequency-diverse aperture for security-screening applications," in *Proc. IEEE Int. Symp. Antennas Propag., USNC/URSI Nat. Radio Sci. Meeting*, San Diego, CA, USA, Jul. 2017, pp. 2383–2384.

[38] D. L. Marks, O. Yurduseven, and D. R. Smith, "Fourier accelerated multistatic imaging: A fast reconstruction algorithm for multiple-input-multiple-output radar imaging," *IEEE Access*, vol. 5, pp. 1796–1809, 2017.

[39] D. L. Marks, O. Yurduseven, and D. R. Smith, "Cavity-backed metasurface antennas and their application to frequency diversity imaging," *J. Opt. Soc. Amer. A, Opt. Image Sci.*, vol. 34, no. 4, pp. 472–480, 2017.

[40] O. Yurduseven, J. N. Gollub, A. Rose, D. L. Marks, and D. R. Smith, "Design and simulation of a frequency-diverse aperture for imaging of human-scale targets," *IEEE Access*, vol. 4, pp. 5436–5451, 2016.

[41] J. N. Gollub *et al.*, "Large metasurface aperture for millimeter wave computational imaging at the human-scale," *Sci. Rep.*, vol. 7, Feb. 2017, Art. no. 42650.

[42] O. Yurduseven, D. L. Marks, T. Fromenteze, J. N. Gollub, and D. R. Smith, "Millimeter-wave spotlight imager using dynamic holographic metasurface antennas," *Opt. Exp.*, vol. 25, no. 15, pp. 18230–18249, 2017.

[43] S. S. Ahmed, *Electronic Microwave Imaging with Planar Multistatic Arrays*. Berlin, Germany: Logos Verlag Berlin GmbH, 2014.

[44] A. Sharma, A. Pedross-Engel, D. Arnitz, C. M. Watts, D. R. Smith, and M. S. Reynolds, "A K-band backscatter fiducial for continuous calibration in coherent millimeter-wave imaging," *IEEE Trans. Microw. Theory Techn.*, vol. 66, no. 1, pp. 431–438, Jan. 2018.

[45] J. Laviada, A. Arboleya-Arboleya, Y. Alvarez-Lopez, C. Garcia-Gonzalez, and F. Las-Heras, "Phaseless synthetic aperture radar with efficient sampling for broadband near-field imaging: Theory and validation," *IEEE Trans. Antennas Propag.*, vol. 63, no. 2, pp. 573–584, Feb. 2015.

[46] D. Smith, O. Yurduseven, B. Livingstone, and V. Schejbal, "Microwave imaging using indirect holographic techniques," *IEEE Antennas Propag. Mag.*, vol. 56, no. 1, pp. 104–117, Feb. 2014.

[47] S. Costanzo, G. D. Massa, M. Pastorino, and A. Randazzo, "Hybrid microwave approach for phaseless imaging of dielectric targets," *IEEE Geosci. Remote Sens. Lett.*, vol. 12, no. 4, pp. 851–854, Apr. 2015.

[48] A. P. Anderson and S. Sali, "New possibilities for phaseless microwave diagnostics. Part1: Error reduction techniques," *IEE Proc. H-Microw., Antennas Propag.*, vol. 132, no. 5, pp. 291–298, Aug. 1985.

[49] K. Wei, "Solving systems of phaseless equations via Kaczmarz methods: A proof of concept study," *Inverse Problems*, vol. 31, no. 12, p. 125008, 2015.

OKAN YURDUSEVEN (S'09–M'11–SM'16) received the B.Sc. and M.Sc. degrees in electrical engineering from Yildiz Technical University, Istanbul, Turkey, in 2009 and 2011, respectively, and the Ph.D. degree in electrical engineering from Northumbria University, Newcastle upon Tyne, U.K., in 2014.

From 2009 to 2011, he was a Research Assistant with the Department of Electrical and Electronic Engineering, Marmara University, Istanbul, Turkey. From 2011 to 2014, he was a Lecturer (part-time) with the Faculty of Engineering and Environment, Northumbria University. From 2014 to 2018, he was a Post-Doctoral Research Associate with the Department of Electrical and Computer Engineering, Duke University, working in collaboration with the U.S. Department of Homeland Security. He is currently a NASA Post-Doctoral Fellow with the Jet Propulsion Laboratory, California Institute of Technology.

He has authored over 80 peer-reviewed technical journal and conference articles and six provisional patents. His research interests include microwave and millimeter-wave imaging, multiple-input-multiple-output radar, wireless power transfer, antennas and propagation, antenna measurement techniques, and metamaterials. He has organized and chaired numerous sessions in international symposiums and conferences, including the IEEE International Symposium on Antennas and Propagation and European Conference on Antennas and Propagation.

Dr. Yurduseven is a member of the European Association on Antennas and Propagation. He was a recipient of an Academic Excellence Award from the Association of British–Turkish Academics, London, in 2013. He was also a recipient of the best paper award at the Mediterranean Microwave Symposium in 2012 and a travel award from the Institution of Engineering and Technology. In 2017, he was awarded a NASA Postdoctoral Program Fellowship administrated by Universities Space Research Association under contract with NASA. In 2017, he was also a recipient of an Outstanding Postdoctoral Award from Duke University and a Duke Postdoctoral Professional Development Award. He was also included in Marquis Who's Who for Excellence in Research in 2017. He serves as a Reviewer for the IEEE TRANSACTIONS ON ANTENNAS AND PROPAGATION, the IEEE TRANSACTIONS ON MICROWAVE THEORY AND TECHNIQUES, the IEEE ANTENNAS AND WIRELESS PROPAGATION LETTERS, the IEEE ACCESS, *Progress in Electromagnetics Research*, and *Applied Physics B*.

THOMAS FROMENTEZE received the Ph.D. degree from the University of Limoges, France, in 2015. From 2015 to 2016, he was a Post-Doctoral Researcher with the CMIP, Duke University, USA. Since 2017, he has been an Assistant Professor with the University of Limoges, where he is currently with the Xlim Research Institute. His main research interests lie in microwave and millimeter wave imaging, computational imaging, wave propagation in complex media, and the associated inverse problems. He was a recipient of the 11th EuRAD Young Engineer Prize during the European Microwave Week 2015.

DAVID R. SMITH (M'98–SM'17) received the Ph.D. degree in physics from the University of California at San Diego, San Diego (UCSD), in 1994. He is currently the Department Chair and James B. Duke Professor of electrical and computer engineering with Duke University and the Director of the Center for Metamaterials and Integrated Plasmonics. He also holds the positions of an Adjunct Professor with the Physics Department, University of California at San Diego, an Affiliate Faculty with the Electrical and Computer Engineering Department, University of Washington, and a Visiting Professor of physics with the Imperial College, London. His research interests include the theory, simulation and characterization of unique electromagnetic structures, including photonic crystals and metamaterials, and applications of such materials.

While at UCSD, he and his colleagues demonstrated the first left-handed (or negative index) metamaterial at microwave frequencies in 2000. He has over 200 publications on matematerials and plasmonics, and was selected by ISI-Reuters as a Citation Laureate in 2009 for the most number of highly cited papers in the field of physics over the last decade. He was once again recognized as one of the Highly Cited Researches 2014 by ISI-Reuters in the category of physics.

In 2002, he was elected a member of The Electromagnetics Academy. In 2005, he was part of a five member team that received the Descartes Research Prize, awarded by the European Union, for their contributions to metamaterials and other novel electromagnetic materials. He was a recipient of the Stansell Research Award from the Pratt School of Engineering, Duke University, in 2005. In 2006, he was selected as one of the Scientific American 50, a group recognized by the editors of Scientific American for achievements in science, technology, and policy. His work has twice appeared on the cover of Physics Today, and twice has been selected as one of the Top Ten Breakthroughs of the year by Science Magazine. In 2013, he was a co-recipient of the James C. McGroddy Prize for New Materials, awarded by the American Physical Society.

In 2006, he along with colleague Sir John Pendry, suggested metamaterials could be used to design an electromagnetic cloak, introducing the new design tool of transformation optics. In 2013, he was asked to write an op-ed piece for the New York Times on cloaking research.

In 2013, he served as a Founding and an Acting Director of the Metamaterials Commercialization Center, a unit within the Intellectual Ventures, Bellevue, WA, USA, dedicated to commercializing metamaterials concepts. MCC has thus far produced three spin out companies: Kymeta Corporation, Redmond, WA, USA, Evolv Technologies, Waltham, MA, USA, and Echodyne, Bellevue, WA, USA. He serves on the Advisory Board for Kymeta, which targets metamaterial-based antennas for satellite communications, and is a Co-Founder of Evolv Technologies, which targets metamaterial apertures for security screening applications, and Echodyne, which is seeking to apply metamaterial apertures to radar applications.

• • •